Heavy-ion resonance and statistical fission competition in the ^{24}Mg+^{24}Mg system at $E_{c.m.}$=44.4 MeV

A. T. Hasan, S. J. Sanders, K. A. Farrar, and F. W. Prosser

Department of Physics and Astronomy, The University of Kansas, Lawrence, Kansas 66045

B. B. Back, R. R. Betts, M. Freer,* D. J. Henderson, R. V. F. Janssens, and A. H. Wuosmaa

Argonne National Laboratory, Argonne, Illinois 60439

A. Szanto de Toledo

Departamento de Física Nuclear, Instituto de Física da Universidade de São Paulo, Caixa Postal 20516, 01498-970 São Paulo, São Paulo, Brazil

The fully energy-damped cross sections of the ^{24}Mg+^{24}Mg reaction at $E_{c.m.}$= 44.4 MeV have been measured for all of the major fission channels. High-resolution Q-value spectra have been obtained for the large-angle yields in the ^{24}Mg+^{24}Mg and ^{20}Ne+^{28}Si channels. Calculations based on the transition-state model are found to reproduce the fully damped cross sections in all of the observed mass channels. The pronounced structure that is observed in the excitation-energy spectra for the more symmetric mass channels, even for the strongly damped yields, is shown to be qualitatively reproduced by assuming a spin-weighted population of the fragment states. There is also evidence, however, that the structure of the nascent fission fragments at scission may influence the population of states in the fragments. These results, taken together with earlier measurements of the resonance behavior of this system, suggest the coexistence of fission from the normal, compact compound nucleus with that from the deformed configurations believed to be responsible for the resonance behavior.

I. INTRODUCTION

The large-angle elastic and inelastic-scattering cross sections for the ^{24}Mg+^{24}Mg reaction at energies near to the Coulomb barrier have been extensively studied because of the striking resonance behavior observed in excitation functions of these yields [1]. Although the origin of the resonance behavior is still a matter of conjecture, several recent measurements support an interpretation in terms of trapping of the ^{48}Cr compound system within a highly deformed, shell-stabilized configuration. As such, the resonance structures can be viewed as the light system analogs to the superdeformed configurations observed in γ-ray studies of medium-mass nuclei (see, e.g., Refs. [2–4]). The evidence for a compound-nucleus origin includes the observation of resonance behavior in the ^{24}Mg(^{24}Mg,^{20}Ne)^{28}Si reaction related to that seen in the inelastic-scattering channels [5] and a spin-alignment measurement for the ^{24}Mg+^{24}Mg resonance at $E_{c.m.}$=45.7 MeV which indicates a very high spin value and, thus, suggests a highly deformed configuration able to sustain this angular momentum [6].

Although the fission of the ^{48}Cr compound nucleus has

been invoked to explain the observed resonance behavior, the relationship between the suggested fission channel, based on very special, deformed configurations of the ^{48}Cr system, and the expected statistical fission of the compound system is not clear. In this context, statistical fission is viewed as the binary decay of the compound nucleus into two fragments, each more massive than the α particle, with the fission probability being determined by the relevant phase space available at the saddle point. The importance of this process in light nuclear reactions has been established in a number of recent measurements and the systematics of the process has been explored in terms of the fission transition-state model [7].

In an attempt to determine the relative significance of these two fission components on the overall cross-section behavior, we have measured the fully energy-damped yields for the ^{24}Mg+^{24}Mg reaction at $E_{c.m.}$=44.4 MeV to all major, observable fission channels. (The ^{8}Be channel is not being considered in this analysis because of its experimental inaccessibility in the present experimental arrangement.) In addition, a coincidence arrangement was employed to obtain high-resolution Q-value spectra for the ^{24}Mg+^{24}Mg and ^{20}Ne+^{28}Si channels where resonance behavior has been observed in excitation-function data. Forward-angle detectors were used to establish the evaporation-residue yields so that the total fusion cross section (leading to evaporation-residue and fission yields) could be characterized. To allow comparison of the transition-state model [7] with the experimen-

---

*Present address: School of Physics and Space Research, University of Birmingham, Birmington B15 2TT, England.

tal excitation-energy spectra, this calculation has been extended to include the known level structure of the symmetric- and near-symmetric-mass fission fragments.

In Sec. II the experimental arrangement is discussed. Following this we present the experimental results for the evaporation residue (Sec. III) and global fission cross-section measurements (Sec. IV), comparing predictions of the transition-state model to the fission results. The high-resolution measurement of Q-value spectra for the symmetric- and near-symmetric-mass fission channels is then presented and a model calculation that is able to describe the main features of these spectra is discussed (Sec. V). The details of this model and its application to the ^{32}S+^{24}Mg fusion-fission reaction, where there is little evidence for heavy-ion resonance behavior, is considered in a companion paper [8]. We conclude with a discussion of the way these results fit in our current understanding of differences between the fission, orbiting, and heavy-ion resonance reaction mechanisms.

II. EXPERIMENTAL ARRANGEMENT

The measurement was performed using the ATLAS facility at Argonne National Laboratory to produce a ^{24}Mg beam of energy 89.0 MeV. Two different ^{24}Mg targets were used, of 40 and 90 μg/cm^2 areal densities, respectively, each supported by 10 μg/cm^2 carbon backings, with the thinner target being of principal importance in obtaining high-resolution Q-value spectra for the more mass-symmetric channels. Center-of-mass energies quoted elsewhere in this paper are calculated for reactions at the respective target centers. A ^{197}Au target was used for energy and solid-angle calibrations and a 170 μg/cm^2 carbon foil was used to establish the contribution of the carbon backing foils to the measurements of fission yields at more forward angles. (It was established that the carbon backings contributed <10% of the yields for all angles and mass channels.) The beam energy was chosen to be sufficiently low to minimize the level of secondary light-particle emission from the fission fragments. This energy is also in the region where extensive studies of the heavy-ion resonance aspects of the reaction have been performed [1,5,6,9,10].

To establish the overall fusion-fission behavior, five Si(Surface Barrier) detectors were located at laboratory angles of 5°, 9°, 15°, 24°, and 35°. (See Fig. 1 for a schematic drawing of the experimental arrangement.) Using the beam timing of the ATLAS facility clear identification of the major "$4n$" channels (^{12}C, ^{16}O, ^{20}Ne, and ^{24}Mg) was achieved with all of the detectors and the three most forward-angle detectors achieved single mass resolution up to $A = 36$. These forward detectors were also used to determine the total evaporation-residue cross section (which is important for comparisons with the fission transition-state calculations [7]). For the evaporation-residue measurement a second setting for the two forward detectors was also employed, with angles of 4° and 8°, respectively. In this second configuration a sixth Si(SB) detector, located at −4°, was also used to help in the determination of the angle offset of the beam through the
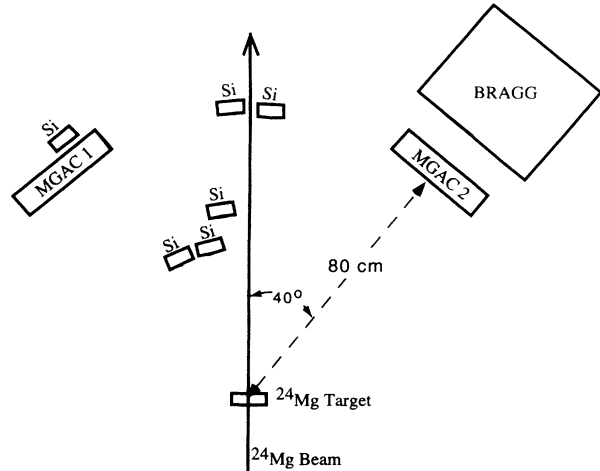

FIG. 1. Schematic diagram of the experimental arrangement. The relative orientations of the detectors are correct, although detector sizes are not to scale.

scattering chamber ($\approx 0.1°$). The advantages in making fission measurements using Si(SB) detectors with time-of-flight mass identification include low energy thresholds and simple efficiency calibrations using elastic-scattering data. These measurements are not suitable, however, for obtaining high-resolution Q-value spectra. Si(SB) detectors achieve only modest energy resolution for heavy ions and also suffer from having a mass and charge dependent pulse-height defect which restricts the accuracy with which they can be calibrated in energy. Cross sections for reaction products measured in the Si(SB) detectors are based on a comparison of the measured elastic-scattering yields in these detectors to the corresponding cross sections calculated using the code PTOLEMY [11].

The high-resolution Q-value spectra for the ^{24}Mg+^{24}Mg and ^{20}Ne+^{28}Si fission channels were obtained by coincidence measurements of the fission fragments using two large-area (20×20 cm^2), position-sensitive, multigrid avalanche counters [12] (labeled MGAC1 and MGAC2 in Fig. 1) located on opposite sides of the scattering chamber at ±40°, 80.5 cm from the target. A mass spectrum of the binary fragments was obtained by measuring the scattering angles of both fission fragments as well as the relative time of arrival of the fragments at the counters. This spectrum is shown in Fig. 2 for the thinner ^{24}Mg target. The abscissa denotes the mass of the fragment detected in MGAC1 located on the opposite side of the scattering chamber to the Bragg-curve detector (see Fig. 1). The asymmetry observed in this figure, with the yield in the $A = 28$ peak about 12% less than that for the corresponding $A = 20$ peak, occurs because of the inefficiency of the MGAC2, in front of the Bragg-curve detector, to detect lower mass fragments. This inefficiency was not found to have a significant Q-value dependence, as determined by comparing the $A = 20$ and 28 spectra, and for cross-section determinations it was possible to correct for the mass dependence of the inefficiency using the data obtained with the Si detector located behind MGAC1.
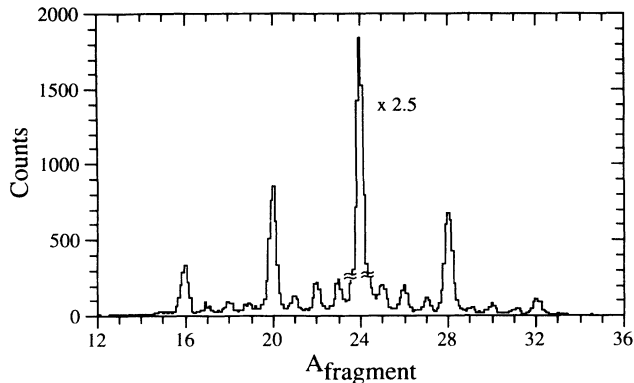
FIG. 2. Mass spectrum obtained from the coincidence measurement of binary-reaction fragments. The abscissa gives the mass of the fragment detected in MGAC1 opposite to the Bragg-curve detector. Note that the $A = 24$ peak has been scaled down to better demonstrate the mass resolution in the other mass channels.

Having established the mass channel, it was then possible to determine the reaction Q-value based solely on the angle measurements. With the timing and position resolution achieved in this measurement ($\Delta t = 400$ ps and $\Delta x = 1.0$ mm) we obtained a mass resolution of 0.6 u (see Fig. 2) and a Q-value resolution for the symmetric $^{24}\mathrm{Mg}+^{24}\mathrm{Mg}$ channel of better than 450 keV, with somewhat lower resolution in the mass-asymmetric channels. A Monte Carlo simulation of the coincidence measurement that reproduces the observed Q-value resolution indicates that the dominant contributions to the energy resolution are the multiple-scattering effects in the target, the size of the beam spot at the target, and, at higher energies, recoil effects resulting from γ-ray emission from the fragments. Thin targets were necessary to keep the multiple-scattering effects to a minimum.

Both of the MGAC's were configured in a transmission geometry with the Si(SB) detector at 35° located behind one of the counters and a large-acceptance, Bragg-curve detector with segmented-anode readout [13] located behind the other. The Bragg-curve detector, which used the MGAC2 counter to determine the scattering angle, was particularly useful in obtaining singles measurements of the fission cross sections leading to the more mass-symmetric channels at the same angles covered by the coincidence measurement. This detector can also be used to determine the isotopic composition of the mass yields. However, the limited dynamic range of the Bragg-curve detector restricted its usefulness for more mass asymmetric channels as fragments with $A \leq 16$ were not fully stopped in the counter. The cross sections deduced from the Bragg-curve detector data were corrected for the trigger inefficiency of the MGAC2 counter, with a maximum correction of 12% applied to the $A = 20$ cross section.

III. EVAPORATION RESIDUES

The evaporation-residue angular distribution for the $^{24}\mathrm{Mg}+^{24}\mathrm{Mg}$ reaction at $E_{\mathrm{c.m.}}=44.4$ MeV is shown in Fig.

3. To obtain this distribution, cross sections corresponding to particles with $A > 34$ were first determined using the forward-angle Si(SB) detectors. This mass region is free from contaminant processes originating from the carbon backing material. The calculated mass distribution of the evaporation residues as a function of angle, found using the computer code LILITA [14], was used to determine the relative contributions to the total angle-dependent evaporation-residue distribution resulting from residues with $A \leq 34$. This correction for the mass distribution, which is included in Fig. 3, ranged from 1.0% in the 4° detector to 7.8% in the 24° detector.

The angle-integrated evaporation-residue cross section was found by scaling the LILITA calculation to the experimental results and then integrating the LILITA distribution, resulting in a total cross section of $\sigma_{\mathrm{ER}}=1065\pm65\pm35$ mb. The first quoted uncertainty reflects how well the LILITA curve reproduces the experimental results. The second uncertainty results from the need to extrapolate the cross section outside of the experimental angular range. This uncertainty was taken as $\Delta\sigma = 0.25\sigma_{\mathrm{LILITA}}(\theta < 4°) + \sigma_{\mathrm{LILITA}}(\theta > 24°)$, with the greater contribution coming from the small-angle extrapolation. The calculated ratio of the total cross section σ_{ER} to the integrated cross section within the experimental range $\sigma(4° \leq \theta_{\mathrm{lab}} \leq 25°)$ was found to be 1.11.

The evaporation-residue cross section deduced from this analysis is compared to previous measurements [15,16] for the $^{24}\mathrm{Mg}+^{24}\mathrm{Mg}$ reaction in Fig. 4. For this figure the uncertainties in the current result have been added in quadrature. The new cross-section result, while at a different energy than the previous experiments, is found to be in good agreement with the systematics es-
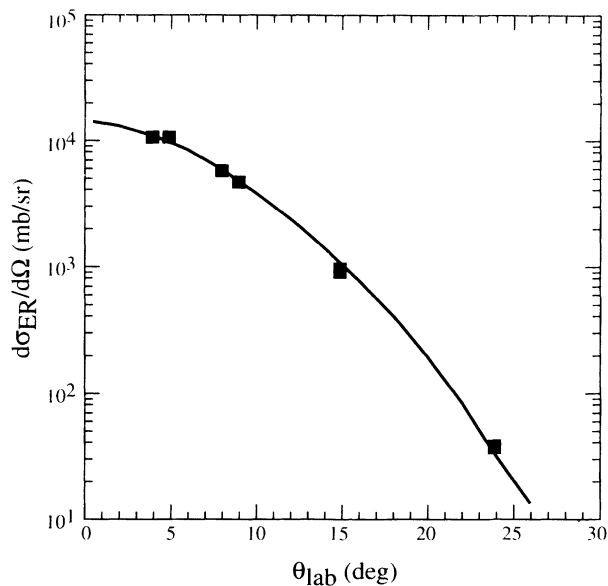

FIG. 3. Evaporation-residue angular distribution for the $^{24}\mathrm{Mg}+^{24}\mathrm{Mg}$ reaction at $E_{\mathrm{c.m.}}=44.4$ MeV. Statistical uncertainties are encompassed by the data points. The curve represents the predicted distribution using the LILITA code, as discussed in the text. This calculation has been scaled to the experimental results.
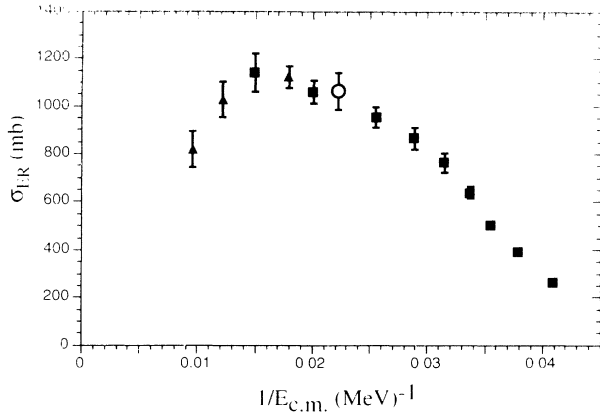
FIG. 4. Evaporation-residue cross section for the ^{24}Mg+^{24}Mg reaction at $E_{c.m.}$=44.4 MeV (open circle). Representative points of Jachcinski *et al.* ([15]) and the results of Prosser *et al.* ([16]) are shown by the solid squares and triangles, respectively.

tablished by these measurements. As seen in the figure, the evaporation-residue cross section may already have reached its saturation value at $E_{c.m.}$= 44.4 MeV.

IV. GLOBAL FISSION SYSTEMATICS

Figure 5 shows the angular distributions $(d\sigma/d\theta)$ for the fission channels. As has been observed in other light systems (e.g., Ref. [17]), the cross sections to the "$4n$" (i.e., $A = 12, 16, 20, 24$, and 28) mass channels are found to be significantly larger than to the other channels. Because of limited counting statistics, we have grouped in sets of three contiguous masses the cross sections for the weaker channels. The mass range $21\le A \le 23$ is not shown since it could only be clearly distinguished from the strong $A = 20$ and $A = 24$ channels in the 24° Si(SB) detector. The open symbols indicate the cross sections determined using the Si(SB) detectors. The angle-averaged cross sections obtained using the Bragg-curve detector (solid symbols) are shown with the angular acceptance of the detector indicated by the horizontal bars. Although the Bragg-curve detector identifies by nuclear charge, rather than by mass, the relative weakness of fission decay to the odd-mass and odd-charge channels makes such a composite figure useful, even though the charge selection is less selective. For masses with $A < 20$ the angular distributions are observed to have a $1/\sin\theta_{c.m.}$ dependence, as expected for the decay of a spinning compound nucleus by fission. For the ^{20}Ne and ^{24}Mg channels the cross sections increase rapidly at more forward angles. This is consistent with deep-inelastic and quasielastic processes dominating the yields in channels near to the entrance channel. Beyond the grazing angle $(\theta_{lab}^{grazing} \cong 19°)$, however, the angular distributions in these channels are also found to follow roughly a $1/\sin\theta_{c.m.}$ dependence. Only the larger angle data are shown for these two channels.

The total cross sections deduced from the angular-distribution data by extrapolating a $1/\sin\theta_{c.m.}$ dependence to the full angular range are shown in Fig. 6. The predictions of the fission transition-state calculation of Ref. [7], including a correction for secondary light-particle emission, are also presented. The transition-state model takes the probability of fission to a given mass channel to be proportional to the density of states above the fission saddle point. In lighter systems the mass-asymmetry dependence of the saddle-point energy favors decay to mass-asymmetric channels, as seen experimentally. For this calculation the fusion partial-wave distribution was taken as

$$\sigma_J = \pi\lambda^2\frac{2J + 1}{1 + \exp\{[J - J_0]/\Delta\}} \qquad (1)$$

with $\Delta = 1\hbar$. The spin-cutoff value J_0 was taken as $30.9\hbar$ to give a total fusion cross section of 1215 mb. This results in reasonably good agreement with both the measured evaporation residue and fission cross sections, with a calculated evaporation residue cross section of 1100 mb and a fission cross section with $A_{fragment} >4$ of 112 mb. Otherwise the parameters of the calculation are fully determined by the overall systematics of fusion and fission
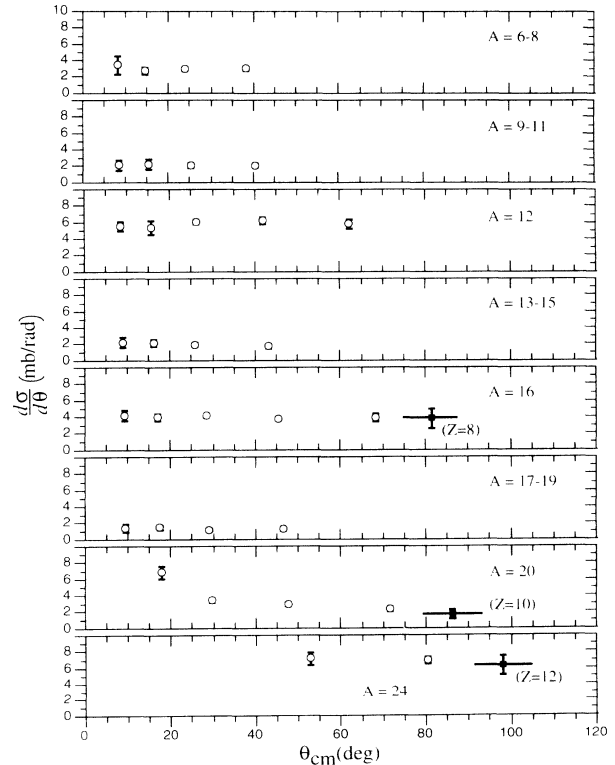

FIG. 5. Angular distributions in $d\sigma/d\theta$ for the fission channels. The open symbols indicate cross sections measured using the Si(SB) detectors. The solid symbols are the corresponding cross sections measured in the Bragg-curve detector, where the identification is in terms of the nuclear charge rather than mass. These latter cross sections are averaged over the acceptance of the Bragg-curve detector, as indicated by the horizontal bars.
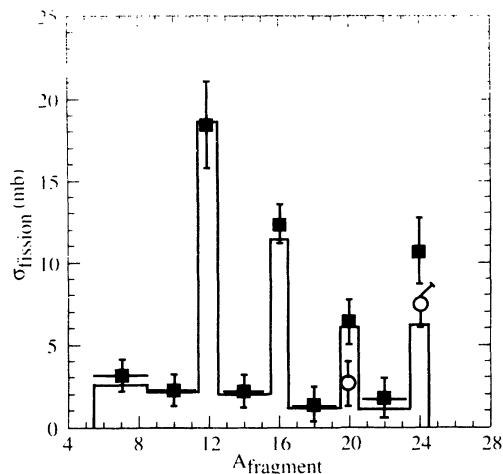
FIG. 6. Angle-integrated cross sections for the fully energy-damped yields. The solid symbols are the cross sections deduced from the singles measurements in the Si(SB) and Bragg-curve detectors, as shown in Fig. 5. For the weaker channels the experimental cross sections are averaged over three contiguous mass channels, as indicated by the horizontal bars. The cross sections deduced from the coincidence measurements, indicated by the open circles, require the coplanarity of the binary fragments with the beam. This requirement selects against events that involve secondary light-particle emission. The predicted cross sections based on the transition-state model and corrected for secondary light-fragment emission, as discussed in the text, are indicated by the histograms using the same binning as the experimental results.
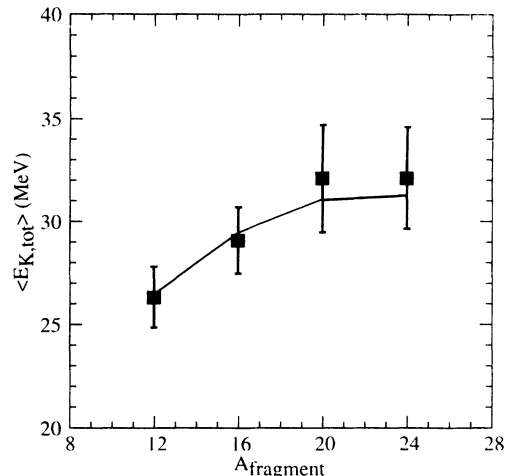
FIG. 7. Average total kinetic energies for the dominant mass channels. The curve connects the predicted energies based on the transition-state calculation assuming equivalent saddle- and scission-point configurations, as discussed in the text.

in light nuclear systems [7]. To compare the calculated and experimental cross sections it is necessary to correct the predicted fission yields to account for the role of secondary light-particle emission. This was accomplished by using the deep-inelastic collision option of the LILITA code [14] to simulate the role of light-particle emission from the fission fragments. At the energy of the present measurement, secondary emission is expected to have little influence on the symmetric ^{24}Mg+^{24}Mg channel, although the low particle threshold of ^{20}Ne does lead to a depletion of yield in this mass channel. The overall excellent agreement of the calculation with the experimental results is in keeping with that found for other systems in this mass range and indicates that the observed cross sections can be understood in terms of the available phase space at the fission saddle point.

Further evidence that the calculation is correctly accounting for the fission phase space and, in particular, for the partial-wave contribution to the fission channels is found in the comparison between the calculated average total kinetic energies in the different mass channels and the measured values, as done in Fig. 7. For the ^{12}C and ^{16}O channels the total kinetic energies are found to be angle independent and, for these channels, the angle-averaged values are indicated. In the ^{20}Ne and ^{24}Mg channels, however, a rapid energy increase is observed at forward angles, again consistent with more periph-

eral reaction mechanisms dominating the forward yields in these channels which are close to the entrance channel. The $\langle E_{K,\text{tot}} \rangle$ values displayed for these channels are from the larger angle data, where both the cross sections $(d\sigma/d\theta)$ and averaged energies are found to be independent of angle.

The final total kinetic energy can be estimated from the model calculations by recognizing that, in lighter systems, the saddle- and scission-point shapes are similar and can be approximated by those of two touching, deformed spheroids [7]. The total kinetic energy of the outgoing fragments is then calculated by assuming that it results from the effective potential energy of the touching spheroids at the saddle point. The angular momentum of the compound nucleus is particularly significant in this calculation since, for light nuclei, it is only for the larger spin values that the relative barriers for fission and light-particle evaporation allow for significant fission competition. The relatively small Coulomb energies and moments of inertia of these systems result in an increased importance for the centrifugal-energy contribution to the observed fragment energies as compared to heavier systems. Again, to compare the calculated total kinetic energies to the experimental results it is necessary to correct for the influence of secondary light-fragment emission, as has been done for the model results presented in Fig. 7 by using the LILITA calculation discussed above. Although the assumption of identical saddle and scission configurations is relaxed in the next section while discussing the model calculation of the excitation-energy spectra (leading to predicted values for $\langle E_{K,\text{tot}} \rangle$ in the symmetric channels about 2 MeV less than shown in Fig. 7), there is still general agreement between the calculated and measured energies.

The agreement between the calculations and the measurements of cross sections and total kinetic energies in

all of the mass channels might be somewhat surprising in view of the strong resonance behavior observed for this system [1]. It should be noted, however, that the resonance effects are only observed at a level of 20–30 % for the higher-lying excitations which dominate the present measurement [6]. At this level the resonance content of the Q-value spectra can be expected to lead to somewhat higher cross sections and kinetic energies than would otherwise be expected, as is seen for the symmetric ^{24}Mg+^{24}Mg channel, but not to the extent of significantly influencing the overall comparisons of the fission model calculations with the experimental results.

V. HIGH-RESOLUTION EXCITATION ENERGY SPECTRA

The excitation-energy spectra for the $A = 20$ and $A = 24$ fission channels, as obtained in the coincidence measurement, are shown in Fig. 8, denoted by the bold line histograms. The Q-value spectra for these channels have been converted to excitation-energy spectra assuming that the ^{20}Ne+^{28}Si and ^{24}Mg+^{24}Mg channels dominate the $A = 20$ and $A = 24$ yields, respectively. (The dominant role of these channels is inferred from the Bragg-curve data as well as from the systematics of fis-
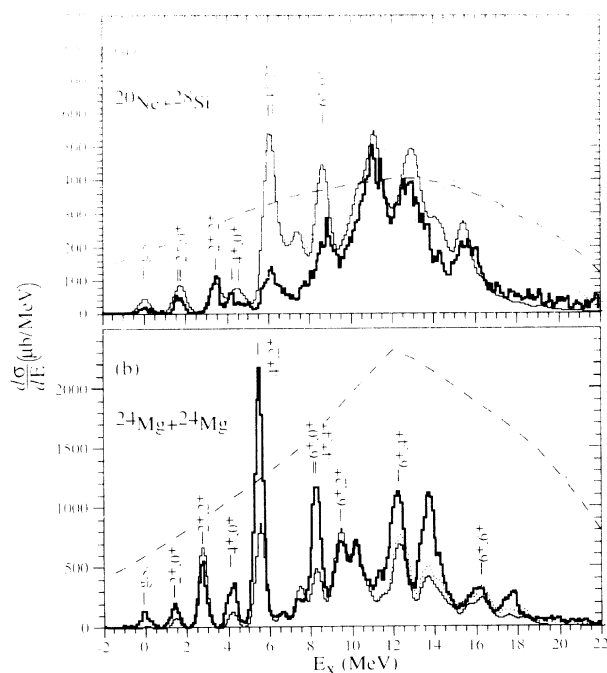

FIG. 8. Excitation-energy spectra for the $A = 20 + 28$ and $24 + 24$ channels. The plots are labeled by the dominant isotopic contribution to each mass channel, as established by the Bragg-curve detector data. These spectra are found by measuring both reaction fragments in the MGAC's. The energy dependence of the efficiency of these measurements is indicated by the dashed curves. The narrow histograms are based on the statistical calculations discussed in the text for all (dotted) and particle-bound (solid) excitations. Locations of single and mutual excitations of yrast states are indicated.
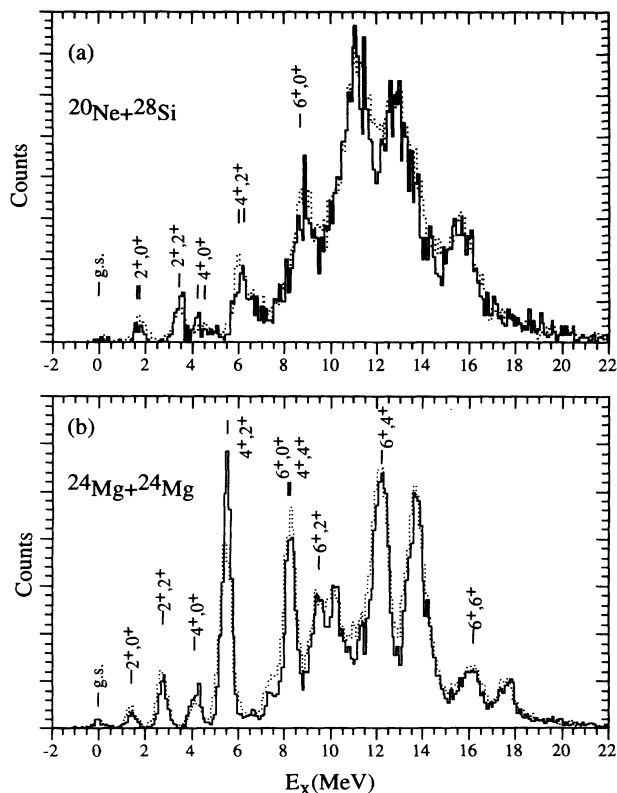
sion in this mass region.) The cross sections were determined using a Monte Carlo simulation of the coincidence efficiency, assuming the $1/\sin\theta_{c.m.}$ angular dependence of the fission fragments. The corresponding detection efficiencies are shown as dashed curves. Neither the ^{20}Ne or ^{24}Mg excitation-energy spectra are found to be limited by the coincidence efficiency. There is, however, a requirement on these spectra that the observed fragments satisfy a coplanarity condition with the beam. This condition effectively discriminates against events involving the secondary emission of light particles and will, therefore, lead to less yield being observed at higher excitation energies as compared to a singles measurement. The angle-integrated cross sections deduced from these data using the Monte Carlo simulation are shown by the open circles in Fig. 6.

It is clear from inspection of Fig. 8 that relatively few mutual excitations dominate the spectra even at the highest energies observed. The high selectivity found in the population of states in the fission decay to the symmetric- and near-symmetric-mass channels was already evident in earlier resonance studies [1,6,10]. Based solely on the number of mutual excitations accessible to the decay of the compound nucleus, a smooth continuum might be expected in the ^{24}Mg+^{24}Mg channel above 10 MeV, where the density of possible excitations reaches a value of 20 MeV^{-1} and increases rapidly with energy. This is clearly an oversimplification, however, as demonstrated in the companion analysis of the ^{32}S+^{24}Mg reaction [8], where the increased statistical weighting of high-spin states of the fragments is seen to lead to significant structures in excitation-energy spectra for the symmetric and near-symmetric fission channels. It has been noted in resonance studies that members of the ^{24}Mg ground-state band play a dominant role in the resonance behavior and this has been suggested to be a consequence of the prolate deformation associated with this band [6]. Excitations built on this band (which are labeled in Fig. 8) are found to be strongly populated, but it is not possible to attribute all of the strong excitations to this band. For example, none of the low-lying 8^+ levels that might represent the continuation of the ground-state band can account for the unidentified peaks in Fig. 8, even though some of these peaks are found to be as strong as the ground-state band excitations. Unfortunately, because of the large number of possible mutual excitations above 10 MeV, it is not possible with the present data to determine the specific excitations responsible for these structures.

A nonresonant origin for the structures observed at higher excitation energy is also suggested by a comparison of the experimental spectra obtained with the thin and thick ^{24}Mg targets. This is shown in Fig. 9(b) where spectra obtained for the ^{20}Ne+^{28}Si and ^{24}Mg+^{24}Mg channels using the two targets are overlaid. These two targets average over incident center-of-mass energies of 160 keV and 365 keV, respectively. Since typical total widths for the resonances observed for this reaction are <200 keV, there should be a significant difference between the spectra for the two targets if the structures arise from a resonant mechanism, assuming all of the structures do not have the same energy dependence. Such

FIG. 9. Comparison of the (a) ^{20}Ne+^{28}Si and (b) ^{24}Mg+^{24}Mg excitation-energy spectra obtained with the thin (solid) and thick (dotted) ^{24}Mg targets. The spectra are scaled and overlaid so as to emphasize differences between the two targets. Locations of single and mutual excitations of yrast states are indicated.

a difference is observed for the $2^+ + 4^+$ mutual excitation of the yrast band, which is known to have a strong resonance energy dependence near this beam energy, but otherwise the spectra for the thin and thick targets are very similar. No significant differences are observed in comparing the thin and thick target spectra for the ^{20}Ne+^{28}Si channel.

To determine the extent that the observed excitation-energy spectra can be understood in terms of the statistical decay of the compound nucleus, the population of specific excitations of the fission fragments was calculated using the procedure detailed in the companion paper on the ^{32}S+^{24}Mg reaction [8]. This calculation, which is based on the transition-state model, distributes the reaction flux calculated for the saddle-point configuration among the possible mutual excitations of the fission fragments based on a statistical spin-weighting of these excitations. The present calculation assumes the same energy difference between the saddle- and scission-point configurations of $\delta = 2.5$ MeV as was used for the ^{32}S+^{24}Mg calculations and is otherwise similar to the earlier analysis. After finding the predicted cross sections for the mutual excitations of the fragments, spectra based on these cross sections were generated by assuming cross-section-normalized Gaussian line shapes for each mutual exci-

tation, taking the Gaussian width as the experimental resolutions of 450 keV and 600 keV for the ^{24}Mg+^{24}Mg and ^{20}Ne+^{32}S channels, respectively. The results of this procedure are shown as the narrow line histograms in Fig. 8. The dotted curves include all known levels in the respective fission fragments, whereas the solid curves require that both of the fragments be populated in particle-bound states. These two curves overlap for lower excitation energies. Although the coplanarity condition used to generate the experimental spectra should minimize the contribution of particle-unbound states to these spectra, there will still be some influence of unbound states at the higher excitation energies. Based on these calculations we expect approximately 40% of the fission events in the ^{20}Ne+^{28}Si channel to populate one or both fragments in a particle-unbound state. In contrast, only about 10% of the ^{24}Mg+^{24}Mg fission events are predicted to populate particle-unbound states.

This highly simplified model is found to reproduce the general characteristics of the measured excitation-energy spectra for the ^{20}Ne+^{28}Si and ^{24}Mg+^{24}Mg channels remarkably well. In both channels, structures appear in the calculated excitation-energy distributions at approximately the same energies as seen in the data and there is good agreement between the centroids of the calculated and measured energy distributions. There are, however, significant discrepancies in the peak cross sections indicating that there is a limit to the degree in which this purely statistical model can account for the experimental results. It also needs to be emphasized that the statistical model is incapable of accounting for the resonances observed for the ^{24}Mg+^{24}Mg reaction that are correlated between the elastic and inelastic channels. Excitation functions calculated using the statistical model can exhibit structure for specific mutual excitations based on a spin-threshold effect resulting from the additional flux available for an excitation as new partial waves become energetically available [18]. However, these thresholds do not occur at common energies and become less important at higher excitation energies where there is competition among a large number of different states.

The energy of the present measurement is close to that where two $J^\pi = 36^+$ resonances have been proposed at $E_{c.m.} = 45.70$ and 46.65 MeV [6,10]. The fission calculation predicts a dominant spin contribution to the ground-state excitation at $E_{c.m.}=44.4$ MeV of $J = 32\hbar$ and, with a calculation closer to the resonance energy, a value of $J = 34\hbar$ at $E_{c.m.}=46$ MeV. This would suggest that the resonance behavior may involve partial waves slightly higher than those dominating the fission process, but not to the extent that competition between the two processes is avoided.

The calculated total cross sections to specific mutual excitations are shown in Fig. 10 for the ^{20}Ne+^{28}Si and ^{24}Mg+^{24}Mg channels. Some of the stronger excitations are labeled by the spins of the constituent states. It is evident from this figure that the structures observed at higher excitation energies in the two channels arise in part from the grouping of high-spin excitations. Very similar behavior was observed for the ^{32}S+^{24}Mg reaction, where the importance of groups of high-spin exci-

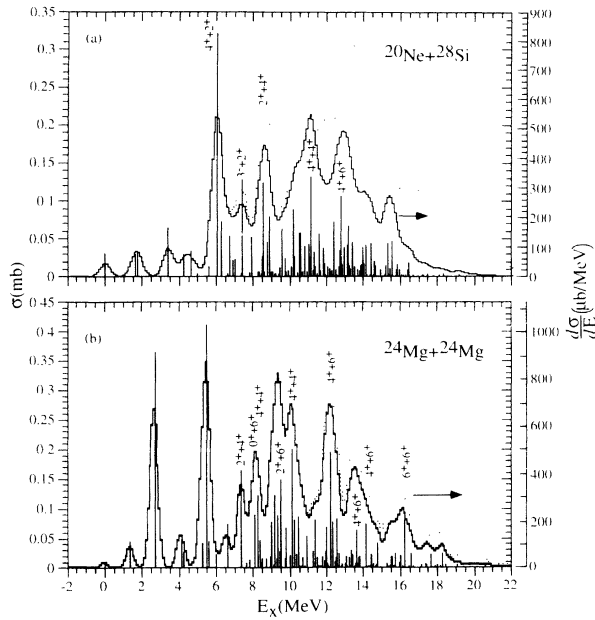FIG. 10. Calculated cross sections for mutual excitations in the (a) ^{20}Ne+^{28}Si and (b)^{24}Mg+^{24}Mg systems. The histograms are the corresponding spectra for all (dotted) and particle-bound (solid) excitations after folding in the experimental energy resolution (scale to right of figure). Spin values for some of the stronger excitations are indicated.

tations on developing structure in the excitation-energy spectra was also suggested by the γ-ray spectra obtained in coincidence with the particle data [8]. The density of mutual excitations in the range 10 MeV$\leq E_x$ $\leq$20 MeV is less with the ^{24}Mg+^{24}Mg reaction as compared to the ^{32}S+^{24}Mg reaction, however, leading to the prediction of more pronounced structure for this lighter system.

VI. DISCUSSION AND CONCLUSIONS

Several conclusions are drawn from the present measurement. First, the overall fission decay from ^{48}Cr is well described by the phase space available at the fission saddle point. Second, as found in other light systems, the mass-asymmetry dependence of the saddle-point energy is seen to favor breakup into the more mass-asymmetric channels. Third, the agreement between the calculated and experimental results, as well as the systematics that have been developed for the fission process in other light systems, suggest that a significant fraction of the fission-like yields observed in the ^{20}Ne+^{28}Si and ^{24}Mg+^{24}Mg

channels arises from this statistical mechanism. We note also that this result is consistent with the observation in resonance studies that the cross sections to higher excitations in these channels show energy fluctuations of only about 20–30 %.

The observation that the fission decay to the ^{20}Ne+^{28}Si and ^{24}Mg+^{24}Mg channels is highly concentrated in only a few mutual excitations is found to be generally consistent with the predictions of a statistical-decay model and are seen to arise from the dominant role of high-spin excitations in the statistical decay. The detailed features in the symmetric- and near-mass-symmetric channels, however, suggest that the structure of the fragments may also influence the fission process. This possibility needs to be explored with particle-γ coincidence measurements, which are planned for the near future.

The present analysis suggests that there may be significant fission contributions even in some of the low-lying excitations where strong resonance features have been observed. This is consistent with the observation of a significant, nonresonant background in excitation functions for these low-lying states. Although the model calculations indicate, on average, that the compound-nucleus spin component leading to these excitations is slightly lower than that inferred from the resonance studies, an interference between the two mechanisms is possible for the higher partial waves leading to fission into these channels. A higher spin component for the resonance behavior than for fission is consistent with the suggestion that the resonances result from a highly deformed configuration of the compound nucleus with a shape similar to that of two end-to-end, ground-state deformed ^{24}Mg particles [6]. This dinucleus configuration would also be consistent with the premise of an "orbiting" model [19,20], and it is possible that the heavy-ion resonance and dinucleus orbiting phenomena are related. The good agreement between calculation and experiment for the more fully damped cross sections suggests that most of this yield arises from the statistical fission of the compound nucleus, with the transition-state phase space determined at the saddle point.

[1] R.W. Zurmühle, P. Kutt, R.R. Betts, S. Saini, F. Haas, and O. Hansen, Phys. Lett. **129B**, 384 (1983).
[2] R.V.F. Janssens and T.L. Khoo, Annu. Rev. Nucl. Part. Sci. **41**, 321 (1991).
[3] P.J. Nolan and P.J. Twin, Annu. Rev. Nucl. Part. Sci.

38, 533 (1988).
[4] P.J. Twin, B.M. Nyakó, A.H. Nelson, J. Simpson, M.A. Bentley, H.W. Cranmer-Gordon, P.D. Forsyth, D. Howe, A.R. Mokhtar, J.D. Morrison, J.F. Sharpey-Schafer, and G. Sletten, Phys. Rev. Lett. **57**, 811 (1986).

[5] S. Saini, R.R. Betts, R.W. Zurmühle, P.H. Kutt, and B.K. Dichter, Phys. Lett. B **185**, 316 (1987).

[6] A.H. Wuosmaa, R.W. Zurmühle, P.H. Kutt, S.F. Pate, S. Saini, M.L. Halbert, and D.C. Hensley, Phys. Rev. C **41**, 2666 (1990).

[7] S.J. Sanders, Phys. Rev. C **44**, 2676 (1991).

[8] S.J. Sanders, A. Hasan, F.W. Prosser, B.B. Back, R.R. Betts, M.P. Carpenter, D.J. Henderson, R.V.F. Janssens, T.L. Khoo, F. Moore, P. Wilts, F.L.H. Wolfs, A.H. Wuosmaa, K.B. Beard, and P. Benet, Phys. Rev. C **49** (1994).

[9] A. Mattis, W. Dünnweber, W. Trombik, A. Glaesner, W. Hering, D. Konnerth, and R. Ritzka, Phys. Lett. B **191**, 328 (1987).

[10] A.H. Wuosmaa, R.W. Zurmühle, P.H. Kutt, S.F. Pate, S. Saini, M.L. Halbert, and D.C. Hensley, Phys. Rev. Lett. **58**, 1312 (1987).

[11] C. Ptolemy, M.H. Macfarlane, and S.C. Pieper, Argonne National Laboratory report, 1978 (unpublished).

[12] F.L.H. Wolfs, Phys. Rev. C **36**, 1379 (1987).

[13] K. Farrar, A. Hasan, F.W. Prosser, S.J. Sanders, and D. Henderson (unpublished).

[14] J. Gomez del Campo, J.A. Biggerstaff, R.A. Dayras, D. Shapira, A.H. Snell, P.H. Stelson, and R.G. Stokstad, Phys. Rev. C **29**, 1722 (1984).

[15] C.M. Jachcinski, D.G. Kovar, R.R. Betts, C.N. Davids, D.F. Geesaman, C. Olmer, M. Paul, S.J. Sanders, and J.L. Yntema, Phys. Rev. C **24**, 2070 (1981).

[16] F.W. Prosser, S.V. Reinert, D.G. Kovar, G. Rosner, G.S.F. Stephans, J.J. Kolata, C.F. Maguire, A. Santo de Toledo, and E. Szanto, Phys. Rev. C **40**, 2600 (1989).

[17] S.J. Sanders, D.G. Kovar, B.B. Back, C. Beck, D.J. Henderson, R.V.F. Janssens, T.F. Wang, and B.D. Wilkins, Phys. Rev. C **40**, 2091 (1989).

[18] R.R. Betts, in *Proceedings of the European Physical Society Topical Conference on Large Amplitude Collective Nuclear Motions*, edited by A. Kiss, J. Nemeth, and J. Zinanyi (Central Research Institute for Physics, Budapest, 1979).

[19] B. Shivakumar, S. Ayik, B.A. Harmon, and D. Shapira, Phys. Rev. C **35**, 1730 (1987).

[20] D. Shapira, R. Novotny, Y.D. Chan, K.A. Erb, J.L.C. Ford, Jr., J.C. Peng, and J.D. Moses, Phys. Lett. **114B**, 111 (1982).